

# Computable Bulk and Interfacial Electronic Structure Features as Proxies for Dielectric Breakdown of Polymers

Deepak Kamal, Yifei Wang, Huan Doan Tran, Lihua Chen, Zongze Li, Chao Wu, Shamima Nasreen, Yang Cao, and Rampi Ramprasad\*



Cite This: <https://dx.doi.org/10.1021/acsami.0c09555>



Read Online

ACCESS |



Metrics & More



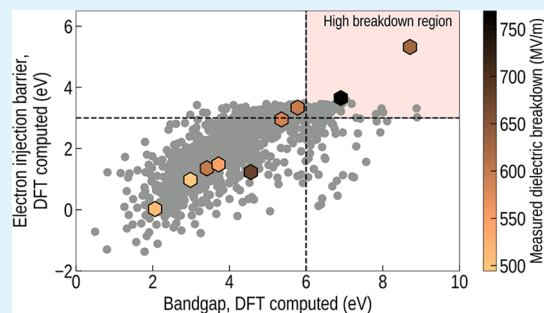
Article Recommendations



Supporting Information

**ABSTRACT:** Breakdown strength, the maximum electric field that can be applied on a dielectric polymer without destroying its insulating characteristics, sets an upper limit on the maximum energy that can be stored in this material. Despite its significance, the breakdown strength remains poorly understood and impractical to compute. This is a major challenge in the development of high-energy dielectric polymers for which a large number of candidates must be screened for identifying those with high breakdown strength. In this work, we develop a multistep strategy for accessing the breakdown strength through two proxies that can be computationally estimated in a high-throughput manner, i.e., the polymer band gap and electron injection barrier at electrode–polymer interfaces. First, these properties are experimentally proven (established) to be correlated strongly with the breakdown strength of a number of benchmark polymers. Then, we develop a simple model, which relies on the chain structure of polymers, to estimate their band gap and electron injection barrier at the level of density functional theory. After validation, this model was finally used for 990 polymers, identifying 53 candidates that have preferable proxies, and thus, potentially having high breakdown strength. Because of the past synthesizability evidence of these polymers, we hope that they may be considered to be synthesized and tested in the near future. Moreover, some empirical rules that were extracted from our computed data could be useful for polymer selection and design in general. We note that the strategy used here is generic and can be used to design materials with other attractive, but complex, properties as well.

**KEYWORDS:** dielectric breakdown strength, polymer, band gap, electron injection barrier, density functional theory, polymer–metal interfaces



## 1. INTRODUCTION

During service life under an electric field, the performance of dielectric polymers will progressively degrade, eventually leading to abrupt failure or dielectric breakdown.<sup>1</sup> The polymer degradation process may involve numerous physical and chemical mechanisms that span multiple time and length scales.<sup>2–4</sup> It was widely believed<sup>5–10</sup> that, among myriads of possible factors, excess charge carriers, which may be injected into and/or generated inside the polymers, play the central role in polymer degradation. Under an external electric field, these carriers can be accelerated, colliding detrimentally with atoms, introducing new atomic-scale damage,<sup>2,3</sup> and generating new charge carriers.<sup>2</sup> When the field exceeds a threshold defined as the breakdown strength  $E_{bd}$ , the charge carrier density and the degree of microscopic damage increases rapidly, ultimately breaking down the material at macroscopic scales. Therefore, factors leading to the presence and the multiplication of charge carriers in the dielectrics may be correlated strongly with  $E_{bd}$ . These factors may serve as “proxies” for  $E_{bd}$  and thus may be used to rationally design high-energy density polymers that display high  $E_{bd}$ .<sup>1,9,11–13</sup>

The polymer band gap ( $E_{gap}$ ) is such a factor that may be correlated with  $E_{bd}$ . Phenomenologically, valence electrons in high  $E_{gap}$  polymers need more energy to be excited, and thus, the charge carrier multiplication and the degradation may be slower and  $E_{bd}$  should ultimately be higher. The correlation between  $E_{gap}$  and  $E_{bd}$  was empirically noted for inorganic solids<sup>1</sup> and has been used for designing high-energy density polymers.<sup>11–14</sup> Another factor that controls the source of the charge carriers is the charge injection barrier at electrode–polymer interfaces, as schematically shown in Figure 1. This figure shows a typical device architecture that involves a polymer film sandwiched within two metal electrodes (Al is used as a prototype metal throughout this work) across which an electric field is applied. Charge carriers (electrons and

Received: May 29, 2020

Accepted: July 24, 2020

Published: July 24, 2020

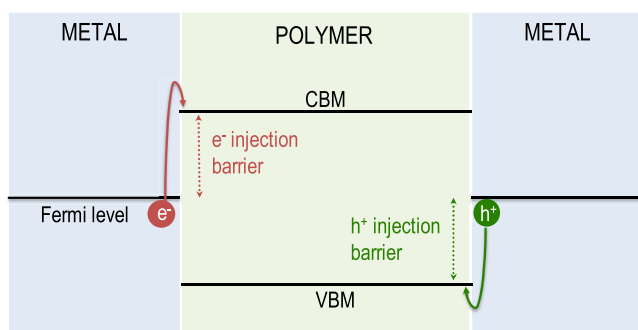


**Figure 1.** Typical polymer–metal interface architecture formed by two metal electrodes and a polymer slab filled between them. Carriers (electrons and holes) from the electrodes are blocked at the metal–polymer interfaces from being injected into the polymer slab by an energy barrier;  $\phi_e$  for electrons and  $\phi_h$  for holes.

holes) from the electrodes are blocked from being injected into the polymer film by a certain energy barrier, i.e., the electron injection barrier ( $\phi_e$ ) and the hole injection barrier ( $\phi_h$ ) where  $\phi_e + \phi_h = E_{\text{gap}}$ . These injection barriers are expected to be correlated to  $E_{\text{bd}}$ .

The charge injection barriers depend strongly on the details of the metal–polymer interface at both microscopic and macroscopic length scales.<sup>15,16</sup> Given the atomic-level model of the interface, these barriers may be calculated using density functional theory (DFT),<sup>17,18</sup> considering various levels of interface details, e.g., the metal and polymer surface orientation and the interface morphology.<sup>16</sup> Such calculations are nontrivial, involving manually constructing the atomic-level metal–polymer models with diverse and relevant microscopic features at the interface and then performing DFT calculations for the generally very large systems. Results obtained from this (computationally very demanding) standard model are in good correspondence with experimental data, as shown in ref 16.

In this paper, we provide direct experimental evidence for the anticipated correlations between  $E_{\text{bd}}$  on one hand and  $E_{\text{gap}}$  and  $\phi_e$  on the other hand for a number of benchmark polymers interfaced with aluminum (Al) electrodes. In other words, we establish that  $E_{\text{gap}}$  and  $\phi_e$  can be used as the proxies for  $E_{\text{bd}}$ . We note that, owing to the relationship between  $E_{\text{gap}}$ ,  $\phi_e$ , and  $\phi_h$ ,

only two of these parameters are independent variables. Thus, in this work, we pick  $E_{\text{gap}}$  and  $\phi_e$  as the two independent quantities. While examining and validating the standard model for computing polymer  $E_{\text{gap}}$  and  $\phi_e$ , we found that they are computationally too expensive for high-throughput screening approaches one may wish to use to identify suitable polymers with high  $E_{\text{bd}}$  values. To address this deficiency, we introduce a simplified method that involves constructing polymer chain models and efficiently computing their electronic properties, which can be used for estimating  $E_{\text{gap}}$  and  $\phi_e$ . Using this method and starting from a set of about 990 previously synthesized polymers and down-select a subset of 53 promising candidates that may be potential high  $E_{\text{bd}}$  polymers. By inspecting the down-selected candidates, chemical design rules for high  $E_{\text{bd}}$  polymers are distilled and discussed. As there is evidence that our candidate set of 990 polymers has been previously synthesized, we hope that the down-selected polymers may be considered for synthesis and testing in the near future.

## 2. METHODOLOGIES

**2.1. Experimental Approaches.** The objective of our experimental work is to establish correlations between potential proxies ( $E_{\text{gap}}$  and  $\phi_e$ ) and the polymer  $E_{\text{bd}}$ . A set of 10 benchmark polymers, including polyamide (KAPTON), polyetherimide (ULTEM), polyether ether ketone (PEEK), polyethylene naphthalate (PEN), polyethylene terephthalate (PET), polystyrene (PS), biaxially oriented polypropylene (BOPP), high density polyethylene (HDPE), nylon-6, and polycarbonate (PC), was chosen for the measurements of  $\phi_e$  and  $E_{\text{bd}}$ .  $E_{\text{gap}}$  of these polymers was collected from the literature.<sup>19</sup>

The experimental setup used to measure  $\phi_e$  is shown in Figure 2a. In the first step, the polymer films were coated with aluminum (Al) using the physical vapor deposition (PVD) method performed with a Denton BenchTop Turbo (BTT). The thickness of the Al coating layers was controlled to be  $\approx 100$  nm. The obtained Al–polymer interface systems were then exposed to an ambient atmosphere for 3 h to reach equilibrium. Next, a voltage bias of 100 V was applied on the sample followed by another equilibration process for 1 h.

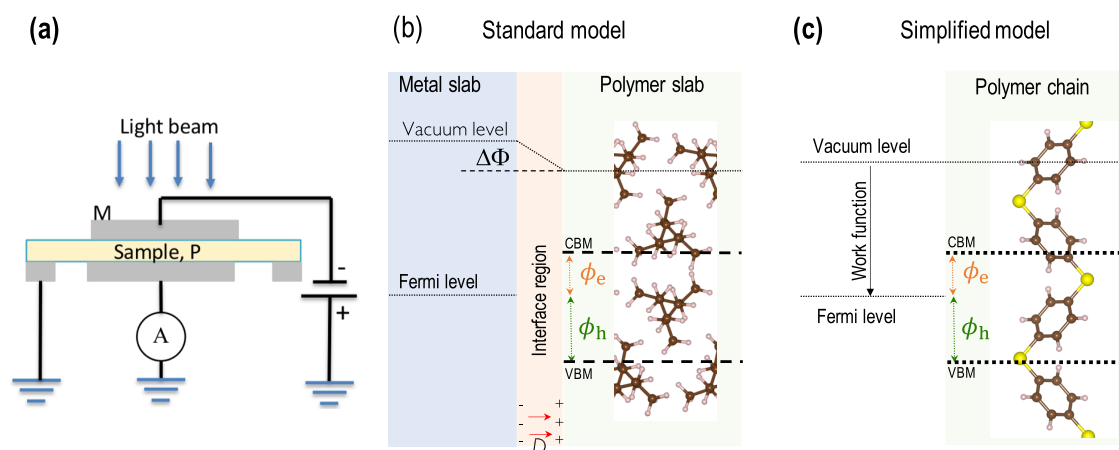


**Figure 2.** (a) Schematic setup for measuring the electron injection barrier from a metal electrode (M) into a polymer film (P). (b) Standard model used to compute  $\phi_e$  and  $\phi_h$  involving a polymer slab interfacing with a metal slab. (c) Simplified model in which only a polymer chain is needed. In panel (b), the interface dipole moment  $D$ , which is indicated by the red arrows, creates the step of  $\Delta\Phi$  of the vacuum level at the interface. Carbon, hydrogen, and sulfur atoms are shown in dark brown, pink, and yellow, respectively.

Photocurrent measurements were carried out using a Fluorolog-3 Horiba Scientific instrument with a Horiba Jobin Yvon double-grating monochromator. A 450 W Xenon short arc lamp with a wavelength range of 200–600 nm was chosen as the light source with a slit width of 10 nm and an increment of 0.1 nm. Current signals were collected by a Model 6514 Keithley electrometer.  $\phi_e$  of the polymer–metal interfaces were obtained from the intercept of Fowler’s plot (photocurrent one/two-incident photon energy). If necessary,  $\phi_h$  may be determined from the experimental band gap  $E_{\text{gap}}$  using  $\phi_h = E_{\text{gap}} - \phi_e$ .

For the breakdown field measurement, the polymer film was placed in between ball-plate electrodes<sup>20</sup> and a positive voltage was applied on the top electrode, while the bottom plate electrode was connected to the ground. A linear voltage ramp of 300 V/s was used to cause dielectric breakdown, and the power supply was shut off after the first breakdown occurred through an interlock with a silicon-controlled rectifier circuit. Weibull analyses followed and involved the fitting of the obtained breakdown probability data to the two-parameter Weibull distribution  $P(E) = 1 - e^{-(E/E_{\text{bd}})^\beta}$  where  $E$  is the electric field created by the applied voltage and  $\beta$  is the shape parameter. In this analysis,  $E_{\text{bd}}$  was determined for a cumulative Weibull distribution of 63.2%.

**2.2. Computational Approaches.** **2.2.1. First-Principles Computation Details.** We computed  $E_{\text{gap}}$  and  $\phi_e$  of the considered models using the DFT formalism, as implemented in the Vienna *Ab initio* Simulation Package (vasp).<sup>21–23</sup> Within this scheme, the Kohn–Sham orbitals were represented using a basis set of plane waves with a kinetic energy of up to 600 eV. The van der Waals dispersion interactions, which are important for describing the interactions at the metal–polymer interface, were estimated with the nonlocal density functional vdW-DF2.<sup>24</sup> Refitted Perdew–Wang 86,<sup>25</sup> the exchange–correlation (XC) functional associated with vdW-DF2, was used for the geometry optimization for which convergence was assumed when the atomistic forces become less than 0.01 eV/Å. The conduction band minimum (CBM), the valence band maximum (VBM), and the band gap of the models were computed using the HSE06 XC functional,<sup>26</sup> the level of DFT needed for reliable results of these important electronic–structure properties.

**2.2.2. Models for the Calculation of  $E_{\text{gap}}$  and  $\phi_e$ .** The advantage of using  $E_{\text{gap}}$  and  $\phi_e$  as proxies to  $E_{\text{bd}}$  is that they can be estimated using reliable computational methods. Typically, such calculations are performed on models involving bulk polymer structures<sup>27</sup> for which the band gap calculation is straightforward. The standard model<sup>16</sup> for computing  $\phi_e$  is schematically described in Figure 2b. If the metal (Al) slab and the polymer slab are separated (i.e., if they do not interact), then  $\phi_e$  and  $\phi_h$  are simply the difference between the CBM or the VBM, respectively, of the polymer slab and the Al Fermi level. The interaction between these slabs introduces an interface dipole moment  $D$ , which shifts the vacuum level of the polymer slab by  $\Delta\Phi = -eD/(2a)$  with respect to that of the metal slab. Having  $\Delta\Phi$  computed using DFT,<sup>16,28,29</sup> the electron injection barrier is then determined using  $\phi_e = E_{\text{F}} - E_{\text{CBM}} + \Delta\Phi$ . In this scheme,  $e$  is the electron charge,  $E_{\text{F}}$  is the position of the Fermi level of the electrode metal, and  $a$  is the area of the interface. In the standard model, experimentally observed interfacial features such as foreign chemical species

and defects can also be considered at a significant computational cost overhead.

It is impractical to perform such sophisticated calculations for a large number of polymers because of several reasons. First, bulk structure information is unavailable for most of the experimentally synthesized polymers. Second, constructing an interface model requires manual and meticulous treatments for each case, leading to laborious and time-intensive calculations. Therefore, we have developed a simplified model, as shown in Figure 2c, for estimating  $E_{\text{gap}}$  and  $\phi_e$  using simple single-chain models of the polymers whose chemical structure may be specified using the simplified molecular-input line-entry system (SMILES). Starting from the polymer SMILES, we used an RDKit toolkit<sup>30</sup> to build up and optimize the monomer “molecular” atomic structures. Then, periodicity was imposed along the chain axis ( $z$  direction) to make infinite polymer chains from the monomers. Along the  $x$  and  $y$  directions, a vacuum region that separates adjacent chains by at least 10 Å was used. The chain model was then optimized using DFT, and the electronic structure was computed using the HSE06 XC functional. From the determined VBM and CBM,  $\phi_e$  can be estimated using a simple procedure. By ignoring the metal–polymer interaction,  $\Delta\Phi = 0$ , and thus, the vacuum levels of the Al slab and the polymer chain are aligned. Then, we determined the position of the Al Fermi level  $E_{\text{F}}$ , which is  $\approx 4.1$  eV (i.e., Al work function) below the vacuum level with respect to the VBM and CBM of the polymers.  $\phi_e$  was then computed directly, as defined above.

The simplified model is computationally efficient because the enormously expensive crystal structure prediction step,<sup>31</sup> which is required for the standard model, is avoided. In spite of the simplicity it offers,  $E_{\text{gap}}$  and  $\phi_e$  calculations are in good agreement with experimental data and those obtained from the standard model, as discussed in the next section. The rationale of this result is that the polymer bulk consists of polymer chains packed together via van der Waals interactions, which are very weak compared to the bonding interactions between atoms in the chains. Therefore, the electronic structure features of polymer bulk are captured well by the polymer chain models.

### 3. RESULTS AND DISCUSSION

#### 3.1. Correlations between Measured Proxies and $E_{\text{bd}}$

Figure 3a shows a clear correlation between the measured  $E_{\text{gap}}$  and measured  $E_{\text{bd}}$  of the polymers considered in this work. This correlation is similar to that noted earlier for inorganic solids,<sup>1</sup> providing the first experimental justification for the use of  $E_{\text{gap}}$  as a screening criterion used recently to discover a host

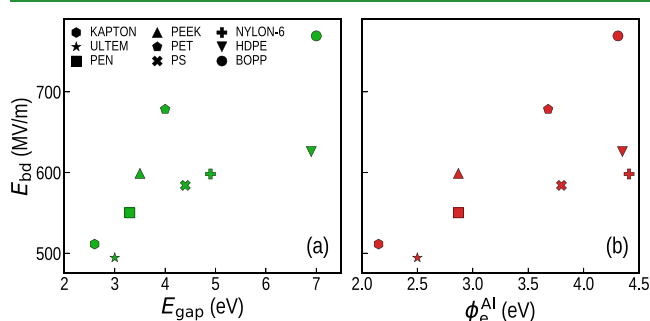


**Figure 3.** Breakdown strength  $E_{\text{bd}}$  measured for 10 Al–polymer interfaces shown as a function of (a)  $E_{\text{gap}}$  and (b)  $\phi_e$ .

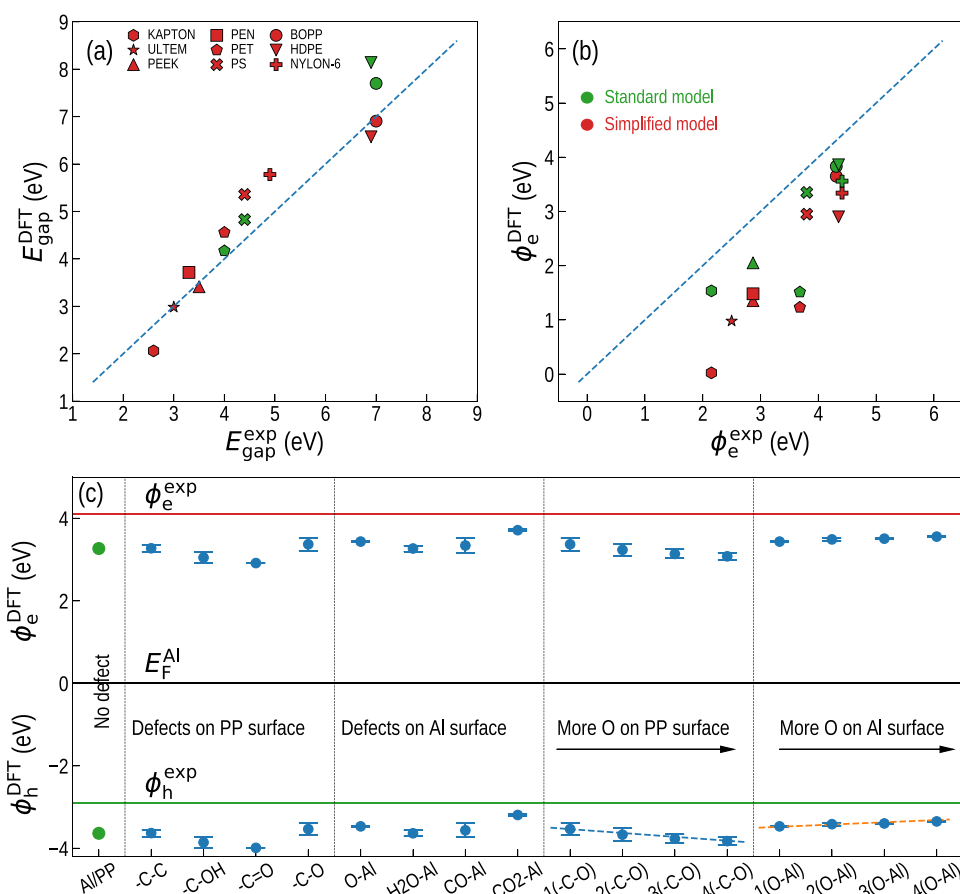


**Figure 4.** (a) Band gap  $E_{\text{gap}}$  and (b) electron injection barrier  $\phi_e$  computed for 10 benchmark polymers and shown in a comparison with experimental values. (c)  $\phi_e$  and  $\phi_h$  are computed for the Al–PP interface using the standard model without (green) and with various interfacial features (blue). Error bars stem from five calculations with different polymer surfaces and arrangements of the interfacial features on each surface model.

of high-energy density polymers.<sup>11,12,14</sup> We also show the measured  $E_{\text{bd}}$  as a function of  $\phi_e$  in Figure 3b. Like with  $E_{\text{gap}}$ ,  $E_{\text{bd}}$  correlates well with  $\phi_e$ . The Pearson correlation coefficients computed for the data shown in Figure 3a,b are 0.77 and 0.73, respectively. Figure 3 implies that  $E_{\text{gap}}$  and  $\phi_e$  can be used as proxies for  $E_{\text{bd}}$  in a large-scale computational screening for potential polymers having high  $E_{\text{bd}}$ , which will be discussed in the next part of this paper.

**3.2. Computed Band Gap and Electron Injection Barriers.** We now evaluate the simplified model in estimating polymer  $E_{\text{gap}}$  and  $\phi_e$ . For this purpose, Figure 4a,b shows  $E_{\text{gap}}$  and  $\phi_e$  computed for the 10 benchmark polymers in comparison with the measured values. Consistent with an early discussion, Figure 4a shows that  $E_{\text{gap}}$  computed using the (simplified) polymer chain model agrees very well with the measured polymer band gap. Similarly, both the standard and simplified models work reasonably well for estimating  $\phi_e$ , capturing the right trend revealed by measurements, as shown in Figure 4b. Some small discrepancies between the standard and simplified models in computing  $\phi_e$  are ascribed to the microscopic details of the metal–polymer interface, which are not captured by the simplified model. The key advantage of this approach over the standard model is that the former requires much less computational cost in computing  $E_{\text{gap}}$  and  $\phi_e$ .

Certain discrepancies between the computed and measured  $\phi_e$  are ascribed to the interface microscopic details, which were

not captured in the “ideal” models whose results are shown in Figure 4b. To examine these factors, Figure 4c shows  $\phi_e$  and  $\phi_h$  calculated using the standard model of the Al–PP interface, considering a variety of interfacial features frequently observed in *in situ* X-ray photoelectron spectroscopy (XPS) characterization experiments and reported literature.<sup>32–36</sup> They are categorized into two groups; the first one includes oxygen atoms with a dangling bond –O–, an oxygen atom with double bonds =O, hydroxyl group –OH, and backbone carbon with a dangling bond –C–. Those in the second group are free oxygen atom O, carbon monoxide CO, carbon dioxide CO<sub>2</sub>, and water molecule H<sub>2</sub>O at the interface. Without defects, the calculated  $\phi_e$  and  $\phi_h$  are about 0.7 eV from the measured values, showing a fairly good agreement. The interfacial features introduced in the model could reduce the discrepancy to as low as  $\approx 0.3$  eV. This is largely related to the polarization of the C–O and Al–O bonds and ultimately to the electronegativity of the oxidant agent O.

**3.3. High-Throughput Screening for High Breakdown Strength Polymers.** According to Figure 3, which reveals the correlations between the proposed proxies and  $E_{\text{bd}}$ , polymers that have high  $E_{\text{gap}}$  and  $\phi_e$  will likely have a high breakdown strength. To exploit these insights, we attempt a high-throughput screening exercise, starting from a set of 990 polymers, as reported to be previously synthesized. The chain models of these polymers were created, and  $E_{\text{gap}}$  and  $\phi_e$  are estimated for the simplified models of Figure 2c. We also

computed the  $E_{\text{gap}}$  and  $\phi_e$  of the 10 polymers whose breakdown strengths were measured in this work. The computed  $E_{\text{gap}}$  and  $\phi_e$  values of all 1000 polymers are shown in Figure 5. The 10 polymers for which experimental values of

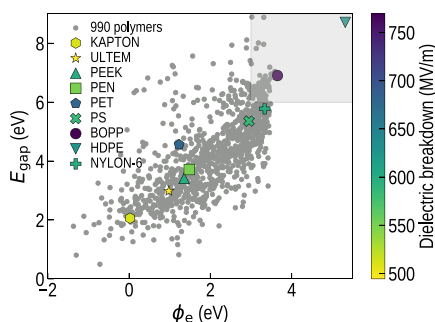


**Figure 5.** Polymer data set of computed  $E_{\text{gap}}$  and  $\phi_e$ . The experimentally measured  $E_{\text{gap}}$  and  $\phi_e$  of 10 polymers considered herein are overlaid to come up with screening criteria to find a polymer with high breakdown. Polymers in shaded areas are predicted to have high  $E_{\text{gap}}$  and  $\phi_e$  and hence, high  $E_{\text{bd}}$ .

$E_{\text{bd}}$  were available are shown using colored symbols with a color representing  $E_{\text{bd}}$  as per the scale in the right of Figure 5. Inspection of five indicates that  $E_{\text{bd}} > 600 \text{ MV/m}$  may necessitate polymers with  $E_{\text{gap}} \geq 6 \text{ eV}$  and  $\phi_e \geq 3 \text{ eV}$ . Using these criteria (indicated by the shaded region on the top right of Figure 5), we identified 53 polymers that potentially could have a high  $E_{\text{bd}}$ . One of these polymers is polyethylene, the common polymer that is well known for its high  $E_{\text{bd}}$  of  $\approx 800 \text{ MV/m}$ . Most of the remaining polymers have been synthesized and reported in some contexts but probably not recognized as high breakdown materials. Because of the past synthesis evidence of the chosen 990 (and the down-selected 53) polymers, we hope that they will be resynthesized and tested for breakdown resistance. A full list of these candidate polymers with details is given in the Supporting Information.

**3.4. Empirical Design Rules.** **3.4.1. Chemical Selection.** A comprehensive inspection on the down-selected polymers (shown in Table S1 of the Supporting Information) reveals some trends in the chemical composition, which could be used as a guideline to identify breakdown resistant polymers. On the one hand, ester bonds, di-ester bonds, amide bonds (peptide bonds), carbamide groups, and aliphatic carbon–carbon (C–C) bonds, which were found frequently, are desirable to achieve high  $E_{\text{bd}}$ . On the other hand, aromatic groups, which are common in popular polymers like PET and PC, are completely absent from the selected list because they significantly reduce  $E_{\text{gap}}$ , thus negatively affecting  $E_{\text{bd}}$ . Such information could be useful for the very early stage of designing/screening polymers with high  $E_{\text{bd}}$ .

**3.4.2. Interface Engineering.** Figure 4c also reveals that charge injection barriers can be tuned by varying the type and the concentration of electronegative species at the metal–polymer interface. Specifically, if we have more O bonded to the PP surface (or Al surface), then  $\phi_e$  is decreased (or increased). This trend difference stems from the direction of the dipole moment involving O. In an Al–O bond, electrons move toward O, creating a dipole moment pointing outward from the Al surface. Similarly, when O atoms are bonded to the polymer surface, the polarity of the C–O bonds also points toward O. The polarities in these two cases are opposite, leading to opposite trends, as shown in Figure 4c. If oxygen is

replaced by a species with higher electronegativity, then the observed trend could be stronger. We note that the electron injection probability scales as  $e^{-\phi_e/k_B T}$  where  $k_B$  is the Boltzmann constant and  $T$  is the temperature; thus, even a small change of  $\approx 0.025 \text{ eV}$  of  $\phi_e$  could change the electron injection probability at room temperature by a factor of 2–3. This effect could be used as a powerful tool for optimizing  $E_{\text{bd}}$  by tuning the electron injection behavior at the metal–polymer interface.

## 4. CONCLUSIONS

In summary, we have combined experimental and computational efforts to develop a reliable strategy for identifying potential polymers that have high breakdown strength  $E_{\text{bd}}$ . The central tenet of this strategy is that the breakdown strength of a polymer when interfacing with a metal electrode correlates strongly with its band gap and the electron injection barrier at the interface. Herein, for the first time, we established these correlations using measured values of  $E_{\text{bd}}$ ,  $E_{\text{gap}}$ , and  $\phi_e$ . These proxies are needed because it is impossible to compute  $E_{\text{bd}}$  while computing  $E_{\text{gap}}$ , and  $\phi_e$  is relatively simple. A computational method is then proposed (and validated) for estimating  $E_{\text{gap}}$  and  $\phi_e$  rapidly and reliably. Using this approach, a high-throughput screening on a set of 990 previously synthesized polymers was performed, uncovering 53 candidates that potentially may display a high electrical breakdown field. We hope that these polymers will go through (re)synthesis and tests for electrical performance. An important broad outcome of this work is a strategy for designing materials with attractive but complex properties (that are difficult to compute or measure) via screening criteria based on easily accessible proxies of the attractive complex property.

## ASSOCIATED CONTENT

### Supporting Information

The Supporting Information is available free of charge at <https://pubs.acs.org/doi/10.1021/acsami.0c09555>.

Contains potential high breakdown polymers identified based on the proxy criterion described in the work (PDF)

## AUTHOR INFORMATION

### Corresponding Author

Rampi Ramprasad – School of Materials Science and Engineering, Georgia Institute of Technology, Atlanta, Georgia 30332, United States; [orcid.org/0000-0003-4630-1565](https://orcid.org/0000-0003-4630-1565); Email: [rampi.ramprasad@mse.gatech.edu](mailto:rampi.ramprasad@mse.gatech.edu)

### Authors

Deepak Kamal – School of Materials Science and Engineering, Georgia Institute of Technology, Atlanta, Georgia 30332, United States; [orcid.org/0000-0003-1943-7774](https://orcid.org/0000-0003-1943-7774)

Yifei Wang – Department of Materials Science and Engineering, University of Connecticut, Storrs, Connecticut 06269, United States; [orcid.org/0000-0002-0848-9977](https://orcid.org/0000-0002-0848-9977)

Huan Doan Tran – School of Materials Science and Engineering, Georgia Institute of Technology, Atlanta, Georgia 30332, United States; [orcid.org/0000-0002-8093-9426](https://orcid.org/0000-0002-8093-9426)

Lihua Chen – School of Materials Science and Engineering, Georgia Institute of Technology, Atlanta, Georgia 30332, United States; [orcid.org/0000-0002-9852-8211](https://orcid.org/0000-0002-9852-8211)

**Zongze Li** – Department of Materials Science and Engineering, University of Connecticut, Storrs, Connecticut 06269, United States

**Chao Wu** – Department of Materials Science and Engineering, University of Connecticut, Storrs, Connecticut 06269, United States

**Shamima Nasreen** – Department of Materials Science and Engineering, University of Connecticut, Storrs, Connecticut 06269, United States; [orcid.org/0000-0002-1504-8555](https://orcid.org/0000-0002-1504-8555)

**Yang Cao** – Department of Materials Science and Engineering, University of Connecticut, Storrs, Connecticut 06269, United States; [orcid.org/0000-0001-7034-2792](https://orcid.org/0000-0001-7034-2792)

Complete contact information is available at:  
<https://pubs.acs.org/10.1021/acsami.0c09555>

## Notes

The authors declare no competing financial interest.

## ACKNOWLEDGMENTS

This work is financially supported by the Office of Naval Research through a Multi-University Research Initiative (MURI) grant (N00014-17-1-2656) and the Toyota Research Institute through the Accelerated Materials Design and Discovery program. Computational resource provided by XSEDE through project “DMR080058N” is also acknowledged.

## REFERENCES

- (1) Huan, T. D.; Boggs, S.; Teyssedre, G.; Laurent, C.; Cakmak, M.; Kumar, S.; Ramprasad, R. Advanced Polymeric Dielectrics for High Energy Density Applications. *Prog. Mater. Sci.* **2016**, *83*, 236.
- (2) Kumazoe, H.; Fukushima, S.; Tiwari, S.; Kim, C.; Huan, T. D.; Kalia, R. K.; Nakano, A.; Ramprasad, R.; Shimojo, F.; Vashishta, P. Hot-Carrier Dynamics and Chemistry in Dielectric Polymers. *J. Phys. Chem. Lett.* **2019**, *10*, 3937–3943.
- (3) Chen, L.; Tran, H. D.; Ramprasad, R. Atomistic Mechanisms for Chemical Defects Formation in Polyethylene. *J. Chem. Phys.* **2018**, *149*, 234902.
- (4) Ieda, M. Dielectric Breakdown Process of Polymers. *IEEE Trans. Electr. Insul.* **1980**, 206–224.
- (5) Von Hippel, A. Electric Breakdown of Solid and Liquid Insulators. *J. Appl. Phys.* **1937**, *8*, 815–832.
- (6) Fröhlich, H. Theory of Dielectric Breakdown. *Nature* **1943**, *151*, 339.
- (7) Fröhlich, H. On the Theory of Dielectric Breakdown in Solids. *Proc. R. Soc. London, Ser. A* **1947**, *188*, 521–532.
- (8) Sawa, G. Dielectric Breakdown in Solid Dielectrics. *IEEE Trans. Electr. Insul.* **1986**, 841–846.
- (9) Ieda, M. Electrical Conduction and Carrier Traps in Polymeric Materials. *IEEE Trans. Electr. Insul.* **1984**, 162–178.
- (10) Ieda, M. Carrier Injection, Space Charge and Electrical Breakdown in Insulating Polymers. *IEEE Trans. Electr. Insul.* **1987**, 261–267.
- (11) Mannodi-Kanakkithodi, A.; Treich, G. M.; Huan, T. D.; Ma, R.; Tefferi, M.; Cao, Y.; Sotzing, G. A.; Ramprasad, R. Rational Co-Design of Polymer Dielectrics for Energy Storage. *Adv. Mater.* **2016**, *28*, 6277–6291.
- (12) Sharma, V.; et al. Rational Design of All Organic Polymer Dielectrics. *Nat. Commun.* **2014**, *5*, 4845.
- (13) Kim, C.; Chandrasekaran, A.; Huan, T. D.; Das, D.; Ramprasad, R. Polymer Genome: a Data-Powered Polymer Informatics Platform for Property Predictions. *J. Phys. Chem. C* **2018**, *122*, 17575–17585.
- (14) Baldwin, A. F.; Ma, R.; Huan, T. D.; Cao, Y.; Ramprasad, R.; Sotzing, G. A. Effect of Incorporating Aromatic and Chiral Groups on the Dielectric Properties of Poly(dimethyltin esters). *Macromol. Rapid Commun.* **2014**, *35*, 2082.
- (15) Friedrich, J. *Metal-Polymer Systems: Interface Design and Chemical Bonding*; John Wiley & Sons, 2017.
- (16) Chen, L.; Huan, T. D.; Quintero, Y. C.; Ramprasad, R. Charge Injection Barriers at Metal/Polyethylene Interfaces. *J. Mater. Sci.* **2016**, *51*, 506–512.
- (17) Hohenberg, P.; Kohn, W. Inhomogeneous Electron Gas. *Phys. Rev.* **1964**, *136*, B864–B871.
- (18) Kohn, W.; Sham, L. J. Self-consistent Equations Including Exchange and Correlation Effects. *Phys. Rev.* **1965**, *140*, A1133–A1138.
- (19) Ohki, Y.; Fuse, N.; Arai, T. Band gap Energies and Localized States in Several Insulating Polymers Estimated by Optical Measurements. *2010 Annual Report Conference on Electrical Insulation and Dielectric Phenomena*; IEEE, 2010; pp. 1–4.
- (20) Treich, G. M.; Tefferi, M.; Nasreen, S.; Mannodi-Kanakkithodi, A.; Li, Z.; Ramprasad, R.; Sotzing, G. A.; Cao, Y. A Rational Co-Design Approach to the Creation of New Dielectric Polymers with High Energy Density. *IEEE Trans. Dielectr. Electr. Insul.* **2017**, *24*, 732–743.
- (21) Kresse, G.; Hafner, J. Ab initio Molecular Dynamics for Liquid Metals. *Phys. Rev. B* **1993**, *47*, 558.
- (22) Kresse, G.; Furthmüller, J. Efficiency of Ab-initio Total Energy Calculations for Metals and Semiconductors Using a Plane-wave Basis Set. *Comput. Mater. Sci.* **1996**, *6*, 15–50.
- (23) Kresse, G.; Furthmüller, J. Efficient Iterative Schemes for Ab Initio Total-energy Calculations Using a Plane-wave Basis Set. *Phys. Rev. B* **1996**, *54*, 11169.
- (24) Lee, K.; Murray, E. D.; Kong, L.; Lundqvist, B. I.; Langreth, D. C. Higher-accuracy Van der Waals Density Functional. *Phys. Rev. B* **2010**, *82*, No. 081101.
- (25) Murray, E. D.; Lee, K.; Langreth, D. C. Investigation of Exchange Energy Density Functional Accuracy for Interacting Molecules. *J. Chem. Theor. Comput.* **2009**, *5*, 2754–2762.
- (26) Heyd, J.; Scuseria, G. E.; Ernzerhof, M. Hybrid Functionals Based on a Screened Coulomb Potential. *J. Chem. Phys.* **2003**, *118*, 8207–8215.
- (27) Huzayyin, A.; Boggs, S.; Ramprasad, R. Density Functional Analysis of Chemical Impurities in Dielectric Polyethylene. *IEEE Trans. Dielectr. Electr. Insul.* **2010**, *17*, 926–930.
- (28) Zhu, H.; Ramprasad, R. Effective Work function of Metals Interfaced with Dielectrics: A First-principles Study of the Pt-HfO<sub>2</sub> Interface. *Phys. Rev. B* **2011**, *83*, No. 081416.
- (29) Cardona Quintero, Y.; Zhu, H.; Ramprasad, R. Adsorption of CH<sub>3</sub>S and CF<sub>3</sub>S on Pt(111) Surface: a Density Functional Theory Study. *J. Mater. Sci.* **2013**, *48*, 2277–2283.
- (30) RDKit: Open-source Cheminformatics. <http://www.rdkit.org>
- (31) Huan, T. D.; Ramprasad, R. Polymer Structure Prediction from First Principles. *J. Phys. Chem. Lett.* **2020**, *11*, 5823–5829.
- (32) Bou, M.; Martin, J. M.; Le Mogne, T.; Vovelle, L. Chemistry of the Interface between Aluminium and Polyethyleneterephthalate by XPS. *Appl. Surf. Sci.* **1991**, *47*, 149–161.
- (33) Dannetun, P.; Boman, M.; Stafström, S.; Salaneck, W. R.; Lazzaroni, R.; Fredriksson, C.; Brédas, J. L.; Zamboni, R.; Taliani, C. The Chemical and Electronic Structure of the Interface between Aluminum and Polythiophene Semiconductors. *J. Chem. Phys.* **1993**, *99*, 664–672.
- (34) Konstadinidis, K.; Papadimitrakopoulos, F.; Galvin, M.; Opila, R. L. In Situ X-ray Photoelectron Spectroscopy Study of Aluminum/Poly (p-phenylenevinylene) Interfaces. *J. Chem. Phys.* **1995**, *77*, 5642–5646.
- (35) Lazzaroni, R.; Brédas, J. L.; Dannetun, P.; Fredriksson, C.; Stafström, S.; Salaneck, W. R. The Chemical and Electronic Structure of the Interface between Aluminum and Conjugated Polymers. *Electrochim. Acta* **1994**, *39*, 235–244.
- (36) Demirkan, K.; Mathew, A.; Weiland, C.; Reid, M.; Opila, R. L. Reactivity and Morphology of Vapor-deposited Al/Polymer Interfaces for Organic Semiconductor Devices. *J. Appl. Phys.* **2008**, *103*, No. 034505.